Microsc. Microanal. 6, 59–67, 2000
DOI: 10.1007/s100059910006

Microscopy AND Microanalysis

Quantitative Short-pulse Acoustic Microscopy and Application to Materials Characterization

Theodore E. Matikas*

Abstract: A new acoustic microscopy method was developed for providing near-surface elastic property mapping of a material. This method has a number of advantages over the traditional V(z) technique. First, it enables one to perform measurements in an automated mode that only requires user intervention in the setup phase. This automated mode makes it feasible to obtain quantitative microscopy images of the elastic property over an area on the material being tested. Also, it only requires a conventional ultrasonic system operating in pulsed mode for collecting the data, rather than a specialized tone-burst system, which is needed in the traditional quantitative scanning acoustic microscopy technique. Finally, unlike the traditional method, the new experimental process does not require calibration of the system's electronics or additional reference data taken under hard-to-duplicate identical conditions from a material that does not exhibit surface acoustic waves.

Key words: acoustic microscopy, materials characterization, nondestructive evaluation

Introduction

Scanning acoustic microscopy (SAM) is a high-resolution nondestructive method useful for near-surface material elastic property quantification as well as crack size determination for surface and subsurface cracks. SAM was developed by Quate et al. (Quate et al., 1979; Quate, 1985) and has been extensively studied by a number of researchers (Weglien and Wilson, 1977; Atalar, 1985; Bertoni, 1985; Gilmore et al., 1986; Liang et al., 1985a,b; Roberts, 1990; Somekh, 1990; Karpur et al., 1993). The most important contrast phenomenon in SAM is the presence of Rayleigh waves, which leak toward the transducer and are very sensitive to local mechanical properties of the material being evaluated (Kushibiki et al., 1982). The generation and propagation of the leaky Rayleigh waves are modulated by the material properties, thereby making it feasible to image even very subtle changes in the elastic properties.

A SAM transducer is schematically shown in Figure 1. The transducer has a piezoelectric-active element situated behind a delay line made of fused silica. The thickness of the active element is chosen to excite ultrasonic signals with a desired nominal frequency when an electrical spike voltage is delivered to the piezoelectric element. In this study, a transducer with a nominal frequency of 50 MHz was selected, although the methodology presented here can be applied to acoustic microscopy lenses of any frequency. The silica delay has a highly focused spherical acoustical concave lens (Fig. 1) that is ground to an optical finish. The numerical aperture (NA; ratio of the diameter of the lens to the focal distance) was 1.25 for the transducer used in this study. A numerical aperture of >1 (or F number—focal

Received April 10, 1999; accepted June 11, 1999.

*Corresponding author, at Orminiou 85, 38222 Volos, Greece.

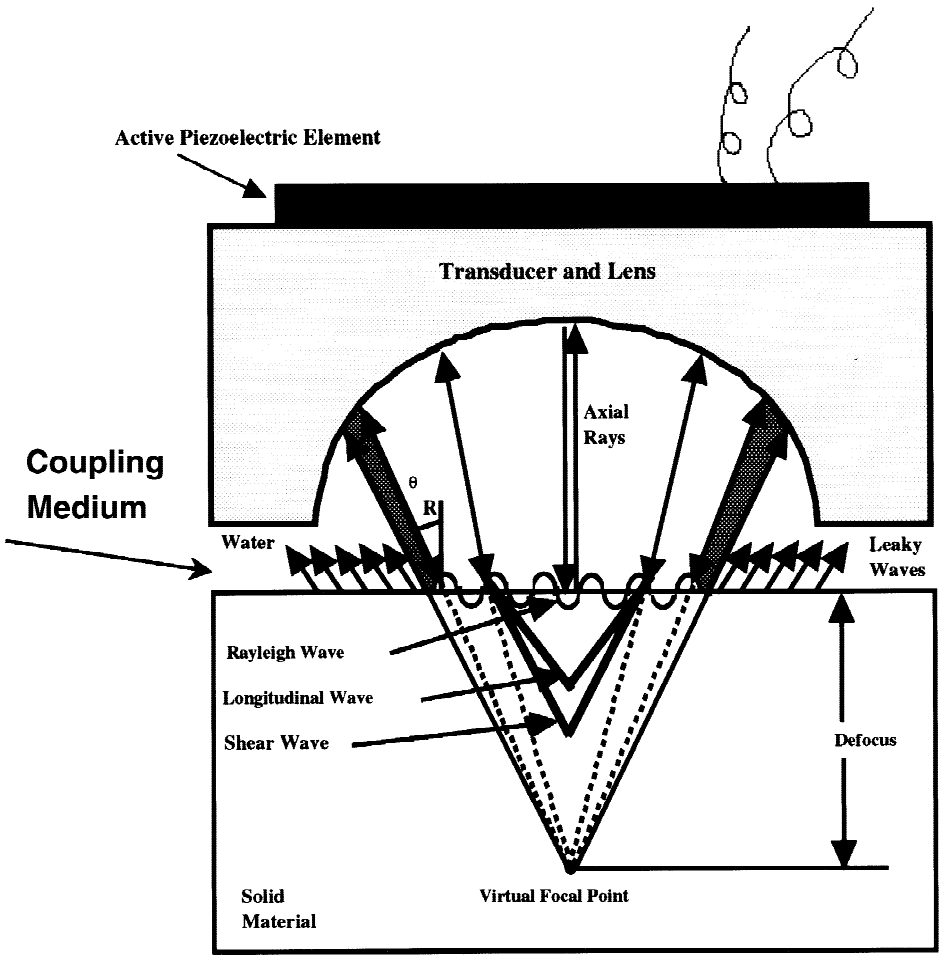

Figure 1. The principle of operation of an acoustic microscope.

distance/diameter—of the lens <1) is essential for the SAM technique to effectively generate and receive surface waves in the sample being imaged. The 50 MHz ultrasonic transducer used in this work had a theoretical focal spot size of approximately 30 μm when focused on the surface of the sample.

The principle of operation of a SAM transducer is based on the generation and propagation of surface acoustic waves (SAW) as a direct result of the high curvature of the transducer's focusing lens and the defocus of the transducer into the sample (Briggs, 1985). The defocus distance also has another important effect on the SAW signal obtained by the SAM transducer. The degree of defocus dictates whether the SAW signal is well separated from the specular reflection or interferes with it. Thus, depending on the defocus, the SAM technique can be used either to map the interference phenomenon in a near-surface layer of the material or to map the surface and subsurface features (reflectors) in the sample.

The mechanism of contrast in the images obtained using a SAM is based on the attenuation and reflection of SAW. In addition, the sensitivity of surface acoustic waves to surface and subsurface features depends on the degree of defocus and has been well documented in the literature as V(z) curves (Kushibiki et al., 1982; Briggs, 1985).

A V(z) curve is obtained when the transducer, kept over a single point, is moved toward the specimen. Then, the signal, rather than simply decreasing monotonically, can undergo a series of oscillations. The series of oscillations at negative defocus can be associated with Rayleigh wave excitation and interaction of a SAW with the specular reflection received directly by the transducer. The Rayleigh wave velocity, v_R, can then be calculated using the following relationship:

$$v_R = v_0 \left\{ 1 - \left[1 - \frac{v_0}{2f.\Delta z} \right]^2 \right\}^{-\frac{1}{2}} \quad (1)$$

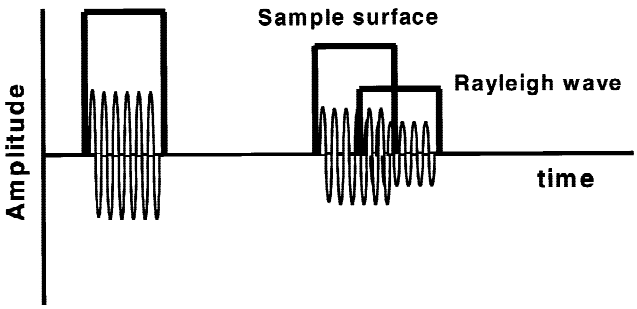

Figure 2. Tone-burst waveform showing the front-surface signal interfering with the Rayleigh wave signal.

Where v_0 is the speed of sound in the coupling medium (water), f is the ultrasonic frequency, and Δz, is the periodicity of the V(z) curve.

The conventional way for measuring SAW velocity is based on a V(z) curve acquisition and analysis procedure developed by Kushibiki and Chubachi (1985). A tone-burst system is used to interrogate the specimen at a specific frequency using specially designed acoustic lenses. In this configuration, the Rayleigh wave and the specular reflection interfere completely, as shown in Figure 2.

The V(z) curve for a specimen under examination is acquired by plotting the amplitude of the tone-burst signal at different defocus depths. Provided a lead response, V_L has been previously obtained for that lens, and the response of the electronic circuit has been calibrated, data for the specimen can now be analyzed. First, V_L is subtracted from V(z). Then, the resulting data are zero padded (extending the record length by adding dummy points of value zero at each end to give adequate resolution in the spatial frequency domain). Finally, a fast Fourier transform (FFT) is performed and the periodicity, Δz, of the V(z) curve is determined. The Rayleigh velocity is then calculated using equation (1).

Methodology for Quantitative Short-pulse Acoustic Microscopy

The new quantitative acoustic microscopy method presented here is based on automated SAW velocity determination via V(z) curve measurements using short-pulse ultrasound. The new method does not require a tone-burst ultrasonic system while it overcomes the limitations of the conventional approach that requires a reference $V_L(z)$ curve and calibration of the electronic circuit of the system. Because the new method is self-calibrated, it can be used for obtaining Rayleigh velocity maps of a specimen through automated V(z) curve acquisition and analysis.

The automated V(z) curve process for SAW velocity measurements can be divided into three basic steps, which are described in detail in the following sections. These steps are:

a. Ultrasonic data are collected using a pulsed acoustic system. The basic data consist of a series of A-scans corresponding to different values of defocus. The waveforms are stored as two different B-scans, one containing the entire signal, the second containing a time-gated portion of the signal that corresponds to specular reflection.
b. The magnitude of the time-gated signal in the Fourier domain is plotted for a selected ultrasonic frequency as a function of defocus distance. This provides a self-calibrated reference $V_R(z)$ curve.
c. The magnitude of the entire A-scan in the Fourier domain is plotted for a specific frequency as a function of defocus distance. The calculated V(z) curve and the reference $V_R(z)$ curve are then processed to compute the Rayleigh velocity of the material at the point where the data were collected.

Data Collection

A conventional pulsed ultrasonic system with a highly focused 50 MHz transducer was used to collect waveforms at different defocus depths. A pair of B-scans from the material under examination was collected. Each B-scan consists of a series of A-scans. The first A-scan in each B-scan is collected with the ultrasonic transducer focused on the surface of the material. The signal is saturated at the front surface, so that the Rayleigh wave is more prominent later in the A-scan. In order to reduce the effects of electrical noise and material induced noise in the signal, about 20 to 25 A-scans were collected at this particular setting and averaged together to form the resulting A-scan. The entire A-scan is stored, as 8-bit data, in the first B-scan, and the time-gated signal of a portion of the A-scan consisting of the specular reflection is stored in the second B-scan. Figure 3 shows the time-gated signal from a fused silica specimen at zero defocus. The waveforms were digitized at 1 nsec/pt using a transducer with a nominal frequency of 50 MHz, but an actual peak frequency of about 30 MHz. The full

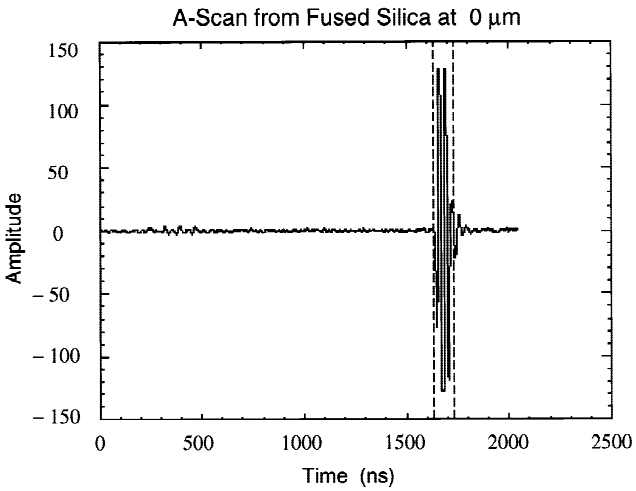

Figure 3. A-scan from a fused silica specimen at zero defocus. A time-gated signal (between dashed lines) containing the specular reflection was acquired.

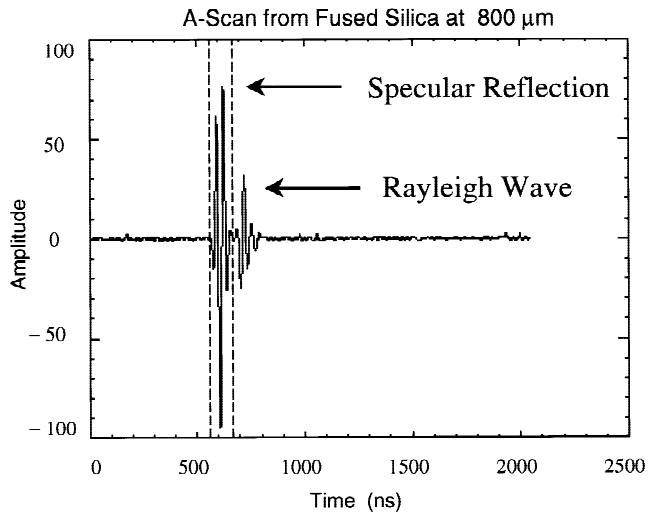

Figure 4. The vertical dashed lines indicate the time-gated portion of the A-scan that corresponds to specular reflection. The waveform was acquired at 800 μm defocus and the Rayleigh wave was separated from the gated specular reflection.

waveforms were 2048 points long. The time-gated portion of the waveform was 104 points.

After the time-gate is set up, the transducer is defocused into the material at a given distance and the A-scan averaging and storage process is repeated for each increment. A total of 1000 A-scans were collected (1 mm total defocus depth for a step size of 1 μm). For small values of defocus, the specular reflection and Rayleigh wave signals overlap one another (Fig. 3). As the defocus distance is increased, the Rayleigh wave separates in time from the specular reflection (Fig. 4).

Reference $V_R(z)$ Curve

A reference curve must be subtracted from the V(z) curve to enable automated calculation of the V(z) curve periodicity. The objective is to remove the effect of the specular reflection and make it possible to use Fourier principle to compute the periodicity. The method used in the conventional technique requires obtaining a $V_L(z)$ curve from a material such as lead that does not exhibit surface acoustic waves. However, this approach also requires using the same transducer and experimental conditions on both the reference material and the material of interest, as well as calibration of the electronic circuit of the system. A manual fit was also used to remove the exponential downtrend in the V(z) data. This alternative procedure is simple but it has a serious limitation since it is difficult to automate the process.

The new method presented here uses the specular reflection signal to construct a reference $V_R(z)$ curve. A software gate is placed to monitor the specular reflection at the same time that a V(z) scan is performed. The magnitude of the geometrical reflection is computed for a selected frequency and then subtracted from a V(z) curve calculated for the same frequency. This method is self-calibrated because the reference curve naturally contains the effect of specular reflection.

As mentioned in the previous section, the first few A-scans collected, which correspond to small defocus distances, have the specular reflection and the Rayleigh wave overlapped in time. In order to obtain a V(z) curve of just the specular reflection, those early A-scans must be ignored. The user can decide how many A-scans must be ignored by either examining the initial B-scan and determining the defocus distance for which the specular reflection and the Rayleigh wave separate in time (Fig. 5) or by looking at an initial V(z) curve and then selecting the appropriate cutoff. The cutoff is based on where the oscillations (due to the Rayleigh wave) die down into the plain exponential curve, which is due to the attenuation of the specularly reflected signal (Fig. 6).

The procedure described above, for removing the unnecessary points, can also be applied in the case of a too wide time-gate containing the specularly reflected signal (Fig. 7). The points that are cut off are then replaced with dummy points. The A-scan at the deepest defocus distance is zero padded at the back-surface end, so that its length is

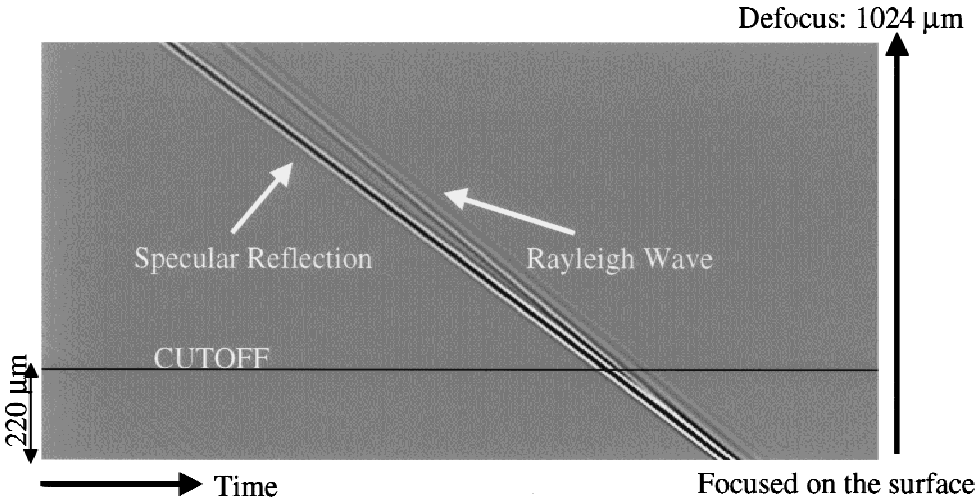

Figure 5. B-scan containing 1024 entire A-scans obtained from a fused silica sample. The increment between A-scans is 1 μm.

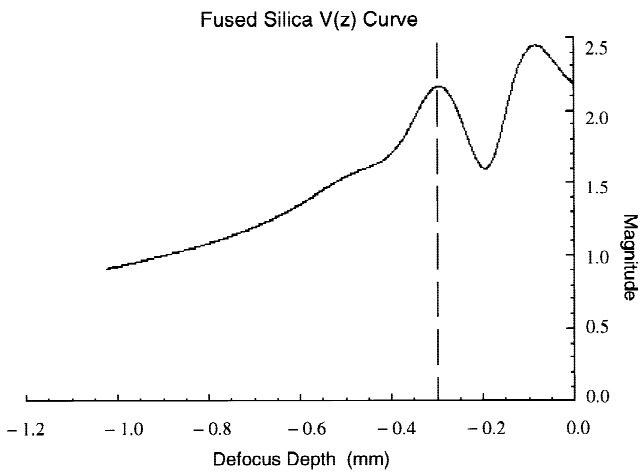

Figure 6. V(z) curve calculated from the time-gated signal (shown in Fig. 3) for fused silica. The dashed vertical line indicates approximately where the specular reflection separates in time from the Rayleigh wave.

the same as an entire A-scan. An FFT is calculated from the padded A-scan, and the frequency of the peak magnitude is identified (Fig. 8). The magnitude at a selected (or peak) frequency plotted as a function of defocus distance forms the $V_R(z)$ curve for the specular reflection signal. The $V_R(z)$ curve is then smoothed with a 51 in length boxcar average, to remove noise and the water ripple from the signal (Fig. 9). The result is finally saved for use in the next processing step.

Material V(z) Curve Obtained from Specimen under Examination

The material V(z) curve if formed in almost the same way as the reference curve. The only difference is that the A-scans are not padded. The selected frequency for calculating the magnitude of the signal in the frequency domain is the same as the one used for constructing the $V_R(z)$ curve. The material V(z) curve is also smoothed with a boxcar average of 51 in width (Fig. 10). Unlike the reference curve, $V_R(z)$, the material V(z) curve exhibits peaks and valleys as the defocus distance changes. These peaks and valleys are due to the constructive and destructive interference in the frequency domain between the specularly reflected and Rayleigh waves.

The resultant V(z) curve at this step is a signal, which oscillates about an exponential; therefore, in its present form, it is difficult to determine its periodicity using an FFT. This problem is alleviated by subtracting the reference $V_R(z)$ curve from the V(z) curve. The V(z) curve then oscillates about a horizontal line (Fig. 11). Next, the first and last 25 points of the resultant V(z) curve are removed, because they are not smoothed, and the result is padded with the average value of the signal to a length of 8192 points, placing half of the padding before the signal and half after it. Note that zero-padding does not work in this case. The FFT of the average-padded V(z) curve is finally calculated and its periodicity is determined (Fig. 12). At this point, any V(z) curve frequencies at or before 2.0E-3 cycles/μm are ignored (Δz = 500 μm and above), as there are not any potential peaks in this area that are related to Rayleigh waves. Any peaks in this area will correspond to FFT noise. The Rayleigh wave velocity is then calculated by using equation (1).

The above-described technique for measuring the Rayleigh wave velocity in a material requires human intervention only in the setup phase, when the user decides how

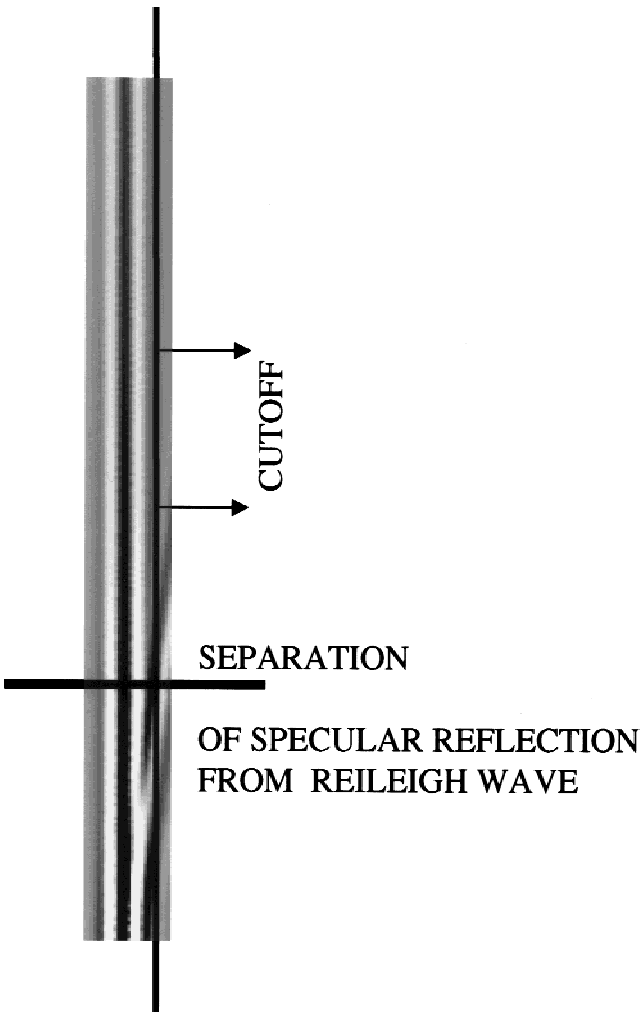

Figure 7. B-scan of the time-gated, specularly reflected signal for fused silica. The horizontal line at 300 μm indicates approximately where the specular reflection and Rayleigh wave separate. Those A-scans pointing to the right of the vertical line are removed before further processing.

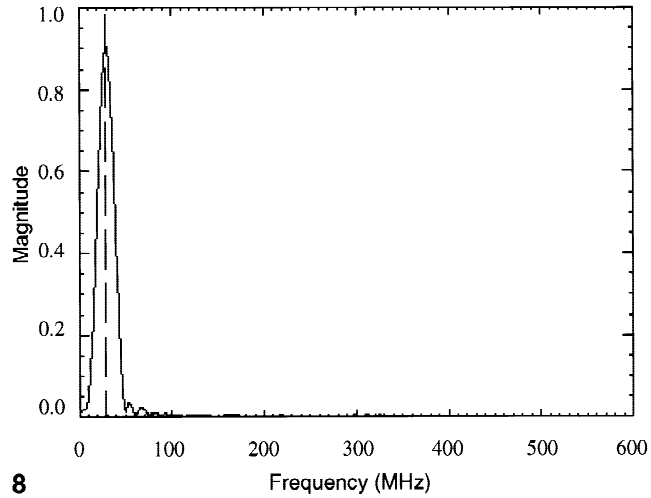

Figure 8. Fast Fourier transform (FFT) of fused silica A-scan at 1023 μm. The entire A-scan is 2048 points long for this data set, so before an FFT is performed, each 104 point–long time-gated A-scan is zero padded to a total length of 2048 points. The central frequency is then determined (dashed vertical line indicates a central frequency of 28.8 MHz).

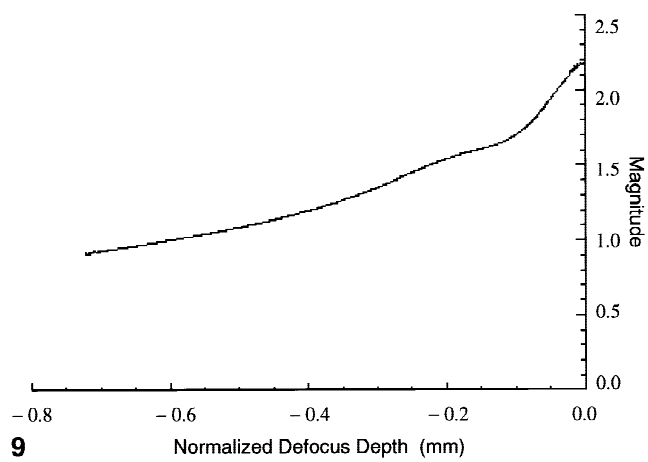

Figure 9. $V_R(z)$ curve of the specular reflection signal from the fused silica sample. Note that the first A-scan used in the analysis was collected from a depth of 300 μm.

many initial A-scans to ignore and when any unnecessary points from the specular reflection A-scans must be removed. As the SAW velocity is determined in a completely automated way, a raster scan over a sample is possible for collecting a pair of B-scans at each point (entire and time-gated waveforms). Then all of the B-scan pairs are processed with user-defined values determined after examining one B-scan at the setup phase. The result is a Rayleigh velocity map over an area on the sample.

Currently, the source code for processing the data is written in PV-Wave (from Visual Numerics, Inc.). Note that the PV-Wave application allows much more user control than is necessary—an ability that was very useful in the development phase of this software.

Application of the Technique for Different Materials

Examples of Rayleigh wave velocity measurements in fused silica and Ti-6Al-4V using the new V(z) procedure are shown next. The fused silica data set presented in Figure 13 has a V(z) curve frequency peak at 3.785E-3 cycles/μm and yields a Rayleigh velocity of 3.44E+3 m/sec. The data set for the Ti-6Al-4V specimen, presented in Figure 14, has a V(z) curve frequency peak at 4.639E-3 cycles/μm and yields a Rayleigh velocity of 3.10E+3 m/sec.

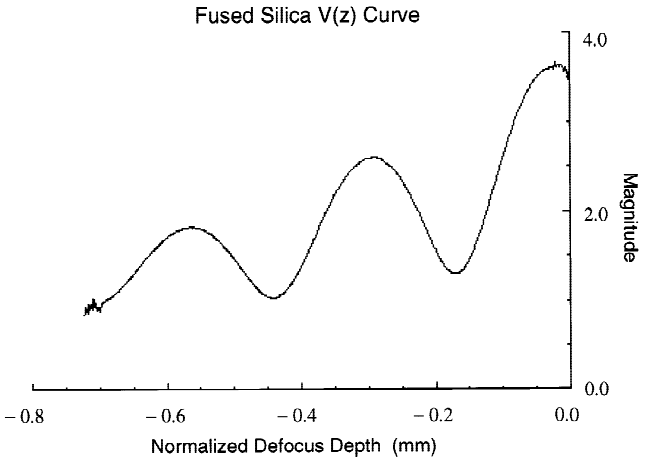

Figure 10. V(z) curve of the entire waveform, after smoothing. The noise at the ends of the curve is due to the smoothing algorithm and is removed before an FFT is calculated.

In the next example, a set of B-scans was collected on an aircraft engine blade sample made from Ti-6Al-4V. This engine blade had been shot-peened in one part of its surface for inducing compressive residual stresses and thereby improving crack initiation and growth resistance. The V(z) curve data were collected along a line on the sample so that about one-half of the data were on the bare Ti-6Al-4V area and the other half on the laser shot-peened area. The increment between each B-scan was 200 μm. Each waveform was 1024 points long, digitized at 2 nsec/pt, and the transducer used was a 50 MHz highly focused ultrasonic transducer. A V(z) curve and the associated Rayleigh velocity were calculated from each B-scan using the automated procedure described here. A one-dimensional map of the Rayleigh wave velocity across the surface of the sample is shown in Figure 15. From this map, the variability in the SAW velocity due to laser shot-peening is clearly observed. Quantitative information on the effect of surface treatment on the local elastic properties of the engine blade was obtained.

Another experiment was performed, this time to determine the calculation error of the technique. A one-dimensional map of the Rayleigh wave velocity was obtained from an E-glass specimen. The E-glass sample was chosen because the SAW velocity was constant along the line of the scan. The SAW velocity calculated along a line on the sample (200 measurements), using the new procedure, ranged from 3099 m/sec to 3116 m/sec. The standard deviation was 6.8 m/sec and the maximum error in SAW velocity compared with the value obtained form time-of-flight measurements was 2.5%.

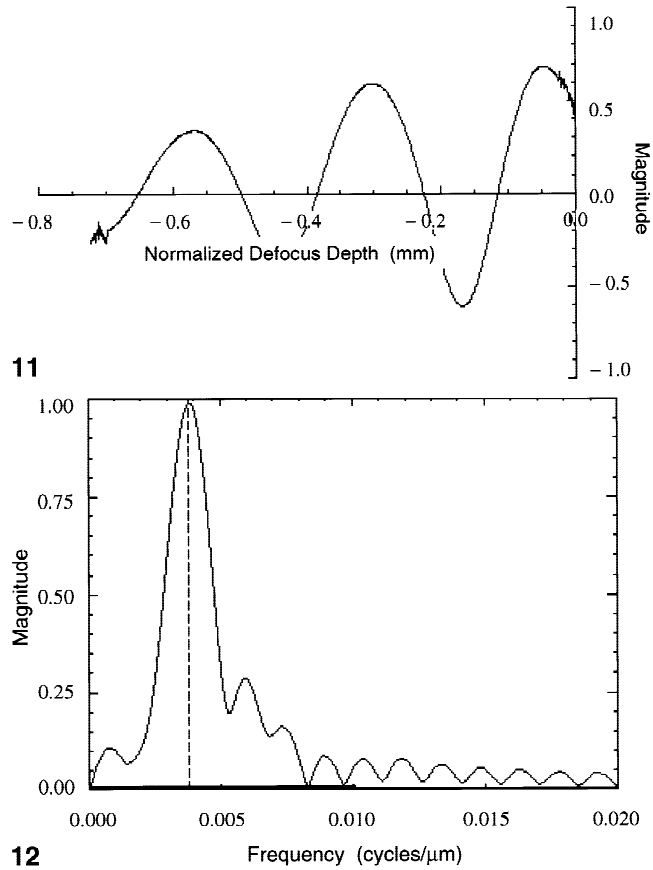

Figure 11. Fused silica V(z) curve after subtraction. After subtracting the specular reflection, $V_R(z)$ curve, from the V(z) curve, the curve oscillates about a horizontal line instead of an exponential.

Figure 12. FFT of fused silica V(z) curve. The dashed vertical line indicates the frequency of the peak, 3.785E-3 cycles/μm, which corresponds to a period Δz = 264.2 μm.

Effect of Defocus Step Size on Accuracy of SAW Velocity Measurement

The accuracy in calculating the Rayleigh wave velocity using the V(z) curve principle generally decreases as the special increment between acquired waveforms along the z-direction increases. In the traditional method, a tone-burst signal of a specific ultrasonic frequency is used and the relationship between defocus step size and accuracy of the measurement follows the general law.

A new method was developed for increasing the accuracy of the SAW wave measurement when coarser defocus steps are used. This method enables one to significantly cut

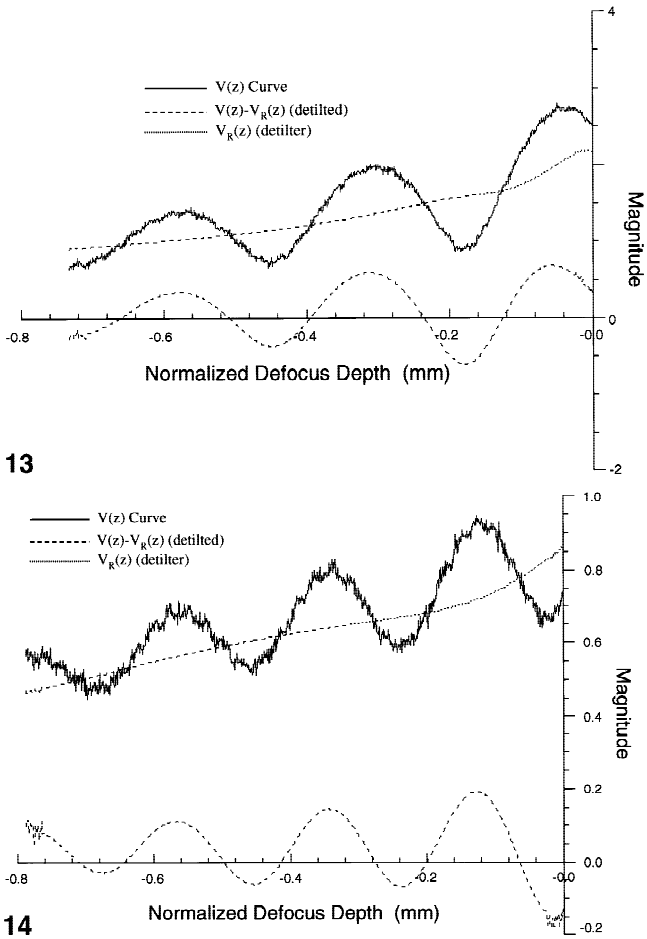

Figure 13. V(z) curve analysis using the new automated procedure for calculating the surface acoustic wave velocity in fused silica.

Figure 14. V(z) curve analysis using the new automated procedure for calculating the surface acoustic wave velocity in Ti-6Al-4V.

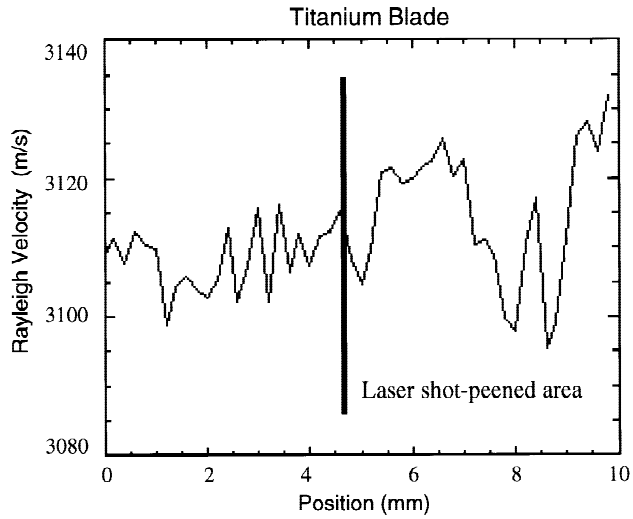

Figure 15. One-dimensional map of surface acoustic velocity in a Ti-6Al-4V engine blade sample with part of its surface laser shot-peened.

the measurement time but maintain high levels of measurement accuracy. The procedure takes advantage of the pulsed excitation used to generate the Rayleigh waves. An FFT is performed on the first A-scan of the B-scan data set used to calculate the V(z) curve, and the central frequency of the signal is determined. The SAW velocity is then calculated, using the new procedure described in the previous sections, for all frequencies about the central frequency with a magnitude above the 6 dB limit. The calculated Rayleigh velocity is finally determined by averaging the values obtained for all the frequencies in the above relevant range.

For a very fine defocus step size, the resultant V(z) curve is of high quality, and the variability in the calculated SAW velocity as a function of selected ultrasonic frequency is small. As the defocus step size increases, the quality of the resultant V(z) curve deteriorates, and the variability in the calculated SAW velocity as a function of selected ultrasonic frequency increases. The accuracy in SAW velocity calculation then decreases because the values of the calculated Rayleigh velocity greatly depend on the ultrasonic frequency used. It is clear from this discussion that using a tone-burst excitation poses a limitation.

In the example shown in Figure 16, an ultrasonic transducer with a central frequency of about 30 MHz was used. The relative range for calculating the SAW velocity was [20,40] MHz. The V(z) curve data were acquired with the finer defocus step size of 1 μm between A-scans. The acquired data were then subsampled by 2, 3, etc. to simulate a defocus step size of 2 μm, 3 μm, etc. The coarser defocus step was 10 μm. Figure 16 shows the variation in SAW velocity measurement as a function of increased defocus step size. Three curves are shown in Figure 16: *curve a* represents the minimum SAW velocity values calculated in the relevant range, as a function of defocus step size; *curve b* represents the maximum SAW velocity values calculated in the relevant range, as a function of defocus step size; and *curve c* represents the average SAW velocity values calculated in the relevant range, as a function of defocus step size. It can be observed that the accuracy of SAW velocity calculations is maintained for defocus step sizes up to 3 μm. This is the limit for acceptable Rayleigh velocity values measured with a tone-burst system. For defocus step sizes >3 μm, the variability in the calculated SAW velocity values

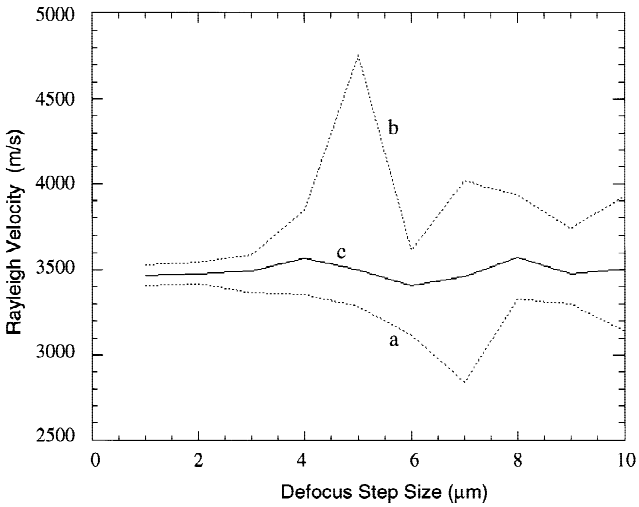

Figure 16. Effect of the defocus step size on the accuracy in Rayleigh wave velocity measurements. a: Minimum values of Rayleigh velocity; b: maximum values of Rayleigh velocity; c: average values of Rayleigh velocity obtained in a relevant frequency range.

dramatically increases when a V(z) curve measurement is performed at a selected ultrasonic frequency (Fig. 16, curves a and b). However, if the new procedure described in this section is used, a high accuracy in Rayleigh wave velocity calculation is maintained even when the defocus step size is dramatically increased (Fig. 16, curve c). It was also found that the method of calculating the SAW velocity based on averaging the values of SAW velocity calculated at different frequencies in the relevant range improves the accuracy of the technique even for the finer defocus step size.

Conclusions

A new quantitative acoustic microscopy technique was developed. The new technique has several advantages over the conventional method. The data can be collected using a pulsed ultrasonic system. The new method does not require the use of a reference material or calibration of the system's electronics to compute the SAW velocity. Measurement of Rayleigh wave velocity is performed in an automated way with user intervention only during the setup phase. Therefore, the new technique enables one to obtain maps of local elastic property over an area of the specimen under examination.

Acknowledgments

This work was supported by and performed on-site at the Materials Directorate, Air Force Research Laboratory, Wright-Patterson Air Force Base, Ohio.

References

Atalar A (1985) Penetration depth of the scanning acoustic microscope. *IEEE Trans Sonics Ultrason* SU-32(2): 164–167

Bertoni HL (1985) Rayleigh waves in scanning acoustic microscopy. In: *Rayleigh-Wave Theory and Application,* Vol. 2, New York: Springer-Verlag; London: The Royal Institution, pp 274–290

Briggs A (1985) *An Introduction to Scanning Acoustic Microscopy, Microscopy Handbooks,* Vol 12. Oxford: Oxford University Press.

Gilmore RS, Tam KC, Young JD, Howard DR (1986) Acoustic microscopy from 10 to 100 MHz for industrial applications. *Philos Trans R Soc Lond* A320:215–235

Karpur P, Matikas TE, Blodgett MP, Jira JR, Blatt D (1993) Nondestructive crack size and interfacial degradation evaluation in metal matrix composites using high frequency ultrasonic microscopy. In: *Special Applications and Advanced Techniques for Crack Size Determination,* Ruschau JJ, Donald JK (eds). Philadelphia: American Society for Testing and Materials, Vol. ASTM STP 1251, pp 130–146

Kushibiki J, Chubachi N (1985) Material characterization by line-focus beam acoustic microscope. *IEEE Trans* SU-32:189–212

Kushibiki J, Ohkubo A, Chubachi N (1982) Effect of leaky SAW parameters on V(z) curves obtained by acoustic microscopy. *Electron Lett* 18:668–670

Liang KK, Bennett SD, Churi-Yakub BT, Kino GS (1985a) Precise phase measurements with the acoustic microscope. *IEEE Trans Sonics Ultrason* SU-32(2):266–273

Liang KK, Kino GS, Khuri-Yakub BT (1985b) Material characterization by the inversion of V(z). *IEEE Trans Sonics Ultrason* SU-32(2):213–224

Quate CF (1985) Acoustic microscopy: recollections. *IEEE Trans Sonics Ultrason* SU-32(2):132–135

Quate CF, Atalar A, Wickramasinghe HK (1979) Acoustic microscopy with mechanical scanning—a review. *Proc IEEE* 67:1092–1114

Roberts RA (1990) Acoustic microscopy for near-surface flaw detection. In: *Elastic Waves and Ultrasonic Nondestructive Evaluation,* Datta SK, Achenbach JD, Rajapakse YS (eds). Amsterdam: Elsevier/North-Holland, pp 445–446

Somekh MG (1990) Theoretical aspects of image formation in the scanning acoustic microscope. In: *Elastic Waves and Ultrasonic Nondestructive Evaluation,* Datta SK, Achenbach JD, Rajapakse YS (eds). Amsterdam: Elsevier/North-Holland, pp 129–134

Weglien RD, Wilson RG (1977) Image resolution of the scanning acoustic microscope. *Appl Phys Lett* 31:793–796